Geophysical Journal International

Geophys. J. Int. (2018) **213,** 181–193
Advance Access publication 2017 December 18
GJI Seismology

doi: 10.1093/gji/ggx544

Fresnel zone in VTI and orthorhombic media

Shibo Xu and Alexey Stovas

Department of Geoscience and Petroleum, Norwegian University of Science and Technology, S.P. Andersens veg 15*a,* 7031 *Trondheim, Norway.*
E-mail: shibo.xu@ntnu.no

Accepted 2017 December 17. Received 2017 November 15; in original form 2017 September 16

SUMMARY

The reflecting zone in the subsurface insonified by the first quarter of a wavelength and the portion of the reflecting surface involved in these reflections is called the Fresnel zone or first Fresnel zone. The horizontal resolution is controlled by acquisition factors and the size of the Fresnel zone. We derive an analytic expression for the radius of the Fresnel zone in time domain in transversely isotropic medium with a vertical symmetry axis (VTI) using the perturbation method from the parametric offset-traveltime equation. The acoustic assumption is used for simplification. The Shanks transform is applied to stabilize the convergence of approximation and to improve the accuracy. The similar strategy is applied for the azimuth-dependent radius of the Fresnel zone in orthorhombic (ORT) model for a horizontal layer. Different with the VTI case, the Fresnel zone in ORT model has a quasi-elliptic shape. We show that the size of the Fresnel zone is proportional to the corresponding traveltime, depth and the frequency. From the numerical examples, we can see that the Shanks transform approximations for Fresnel zone are very accurate for both VTI and ORT media.

Key words: Acoustic properties; Seismic anisotropy; Wave propagation.

INTRODUCTION

The most common question in the reflection seismology is the resolution of the seismic image. We can consider both vertical and horizontal resolution. The horizontal resolution is controlled by acquisition factors and the size of the Fresnel zone. The Fresnel zone is, named for physicist Augustin-Jean Fresnel, used to compute the radio waves propagating between a transmitter and a receiver in antenna system (Hristov 2000). The Fresnel zone or first Fresnel zone in geophysics indicates the portion of a reflector from which the energy of a reflection can reach a detector where the wave propagates within a 1/4 wavelength. The second Fresnel zone is defined from the energy that arrives delayed one-half to one cycle, adding destructively to the energy from the first zone. Similarly, there is a third zone and so on. The adjective 'first' is often dropped away because when the contributions of all zones are added together, only the first Fresnel zone remains while the effects of all subsequent zones cancel each other. Borrowed from classical physical optics, Seismic interpreters often use the Fresnel-zone concept to estimate the lateral resolution of unmigrated, stacked *P*-wave data. (Lindsey 1989; Sheriff 1996).

The Fresnel zone can be defined as the region of constructive interference enclosing the ray-theoretical reflection or mode-conversion point (Sheriff 1980). Fresnel zones and volumes can be computed very efficiently by forwarding dynamic ray tracing in a known velocity model (Červený & Soares 1992). Eaton *et al*. (1991) extended the Fresnel-zone concept to include mode-converted (*P–SV*) reflections for both surface and VSP geometries. The equation that describes the size of a Fresnel zone in a constant-velocity medium for a zero offset can be found in (Sheriff 1996). How actual Fresnel zones are computed for 3-D zero-offset reflections by forwarding modelling in a known medium is described in Hubral *et al.* (1993).

The projected Fresnel zone of a zero-offset reflection onto the subsurface reflector using a standard 3D CMP traveltime analysis, without knowing the overburden was developed in (Hubral *et al.* 1993; Schleicher *et al.* 1997). The calculation for the Fresnel zone radius was done in the time domain by Trorey (1970).

Since the Fresnel zone width is a measure of lateral resolution, usually, seismic waves cannot detect the subsurface features smaller than the size of Fresnel zone. More attention has been made to the awareness of three-dimensional effect within the frame of seismic resolution. Aspects of the seismic resolution which can be achieved in a seismic survey and the physical factors that limit this resolution have been treated by Sheriff (1980) and Lindsey (1989). The Fresnel zone determines the spatial resolving power for unmigrated seismic data with which important lithological changes along a seismic profile direction may be observed (Sheriff 1980). Additionally, it also largely contributes to the reflected and transmitted wavefields, and more specifically to their amplitudes (Spetzler & Snieder 2004; Favretto-Cristini *et al.* 2007a,b). Hagedoorn (1954) pointed out that the reflections area of the interface, and therefore vertical resolution can also be thought of as a Fresnel-zone problem. While the vertical resolution is mostly linked to the seismic wavelength (see, for instance, Widess 1982), the lateral resolution depends on Fresnel zone considerations (Lindsey 1989) and its difference in pre- and

post-migrated data. Červený (2001) suggests two methods to include the Fresnel zone parameter calculations into the ray tracing procedure in complex 2D and 3D structures. Using a derivation that is based on mostly geometric considerations, Monk (2010) examined the shape of the Fresnel zone for the nonzero offset for a model with constant velocity gradient. The implications for seismic acquisition for adequate imaging were made by Monk (2009) when the Fresnel zone is properly sampled.

Few papers have been devoted to anisotropic media. For instance, Okoye & Uren (2000) calculate the Fresnel zone radius for zero-offset configurations for *P*- and *SH*-waves in TI media and isotropic media and for dipping plane reflectors. They conclude that the Fresnel zone radius is predominantly dependent on the curvatures and wavelength of the wave front as well as the dip angle of the reflector. The Thomsen anisotropy parameters δ, ε and γ (Thomsen 1986) also affect the Fresnel zone radius. Moser & Červený (2007) show how the Fresnel region can be calculated by conventional dynamic ray tracing in Cartesian coordinates, for isotropic and anisotropic inhomogeneous layered media. Fresnel volume and interface Fresnel zone for reflected and transmitted waves from a curved interface in anisotropic media were analysed by Ursin *et al*. (2014).

In this paper, an analytic expression for the Fresnel zone radius is derived using the traveltime for VTI model by using the perturbation method. In order to do that, the parametric offset-traveltime equations under the acoustic approximation are used. We apply the Shanks transform to stabilize the approximation and improve the accuracy. The similar perturbation strategy is applied for the analytic expression of Fresnel zone radius in orthorhombic (ORT) model. The accuracy of proposed approximation for Fresnel zone is illustrated for both VTI and ORT models.

FRESNEL ZONE USING THE TRAVELTIME

The seismic wave sent out from the source propagates in space and spread out over a larger area. The horizontal resolution is controlled by the Fresnel zone, the part of a reflector covered by the seismic signal at a certain depth where the wave propagates within 1/4 wavelength after it first touches the reflector. The Fresnel zone (or first Fresnel zone) radius for a homogeneous horizontal layer is defined in Fig. 1 (top). It is convenient to express the Fresnel zone using the traveltime parameters. The Fresnel zone radius X_F can be treated as the wave propagates in lateral direction with certain traveltime t_F and the Fresnel zone radius using the traveltime is calculated by using the Pythagorean theorem (Fig. 1, bottom),

$$X_F^2 + Z^2 = \left(V_\phi t_F\right)^2, \tag{1}$$

where t_F is the corresponding traveltime when the wave propagates by 1/4 wavelength after arriving the reflector with $t_F = t_0 + \Delta t$, where $\Delta t = \frac{1}{4f}$, f is the frequency, t_0 is the vertical traveltime with $t_0 = \frac{Z}{V_0}$, Z is the reflector depth, V_0 is the *P*-wave vertical velocity, V_φ is the corresponding group velocity computed for group angle φ defined from the vertical axis.

For a horizontal layer in a homogeneous isotropic (ISO) medium ($V_\varphi = V_0 = V$), the Fresnel radius using the traveltime is computed as following

$$X_F = V\sqrt{t_F^2 - t_0^2}. \tag{2}$$

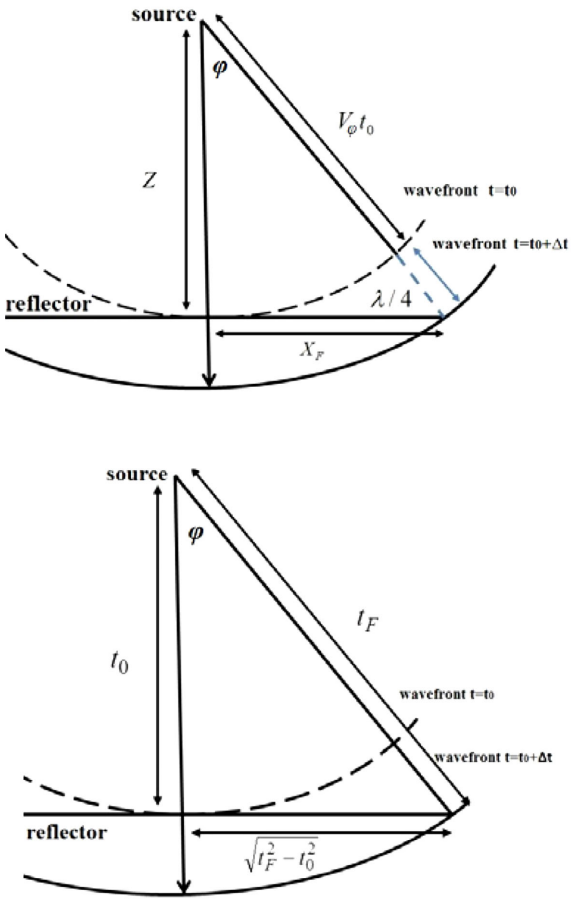

Figure 1. The first Fresnel zone diagram in represented by the depth (top) and traveltime (bottom).

By using $t_F = t_0 + \frac{1}{4f}$, the radius of Fresnel zone X_F can be computed from simple geometrical considerations (Fig. 1, top),

$$X_F^2 + Z^2 = \left(t_0 V + \frac{\lambda}{4}\right)^2, \tag{3}$$

where λ is the wavelength with $\lambda = \frac{V}{f}$, V is the constant velocity. Solving eq. (3) for X_F gives

$$X_F = \sqrt{\left(Z + \frac{V}{4f}\right)^2 - Z^2}. \tag{4}$$

As the wave propagates in three dimensions, the Fresnel zone for the isotropic model above is a circle with the radius computed from eq. (4) shown in Fig. 2.

THE FRESNEL ZONE IN A VTI MEDIUM

In an anisotropic medium, the velocity of the seismic wave varies with the propagation angle. For a homogeneous VTI model, there are two additional anisotropic parameters δ and ε (Thomsen 1986). The shape of the *P*-wave wave front in VTI model is a quasi-ellipse instead of a circle as it is shown in Fig. 3.

Based on the concept of the Fresnel zone, which indicates the area in the vicinity of a ray that can be expressed in terms of the traveltime (t_F) (Fig. 1, bottom) and the change in this traveltime with one-fourth of the wavelength (Δt). Computed from the dynamic ray tracing, the parametric equations for traveltime and offset are given

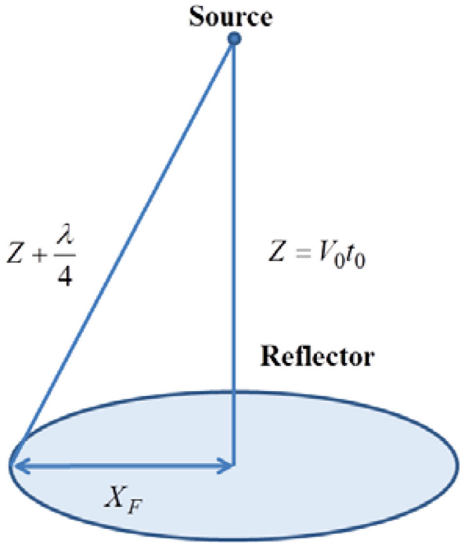

Figure 2. The diagram showing the Fresnel zone in an isotropic medium.

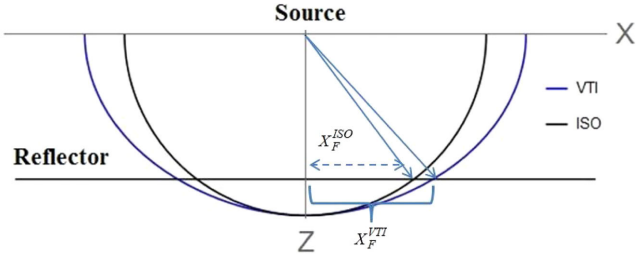

Figure 3. The radius of Fresnel zone for *P* wave in homogeneous ISO and VTI media.

by (Alkahlifah 1998)

$$x(p) = \frac{pt_0V_n^2}{\left(1-2\eta p^2V_n^2\right)^{3/2}\sqrt{1-(1+2\eta)\,p^2V_n^2}},$$
$$t(p) = \frac{t_0\left(2\eta p^4V_n^4+\left(1-2\eta p^2V_n^2\right)^2\right)}{\left(1-2\eta p^2V_n^2\right)^{3/2}\sqrt{1-(1+2\eta)\,p^2V_n^2}}, \tag{5}$$

where V_n is the normal moveout (NMO) velocity with $V_n = V_0\sqrt{1+2\delta}$, $\eta = \frac{\varepsilon-\delta}{1+2\delta}$ is the anellipticity parameter (Alkhalifah & Tsvankin 1995), and p is the ray parameter (horizontal slowness). For the Fresnel zone in VTI model, the radius is computed from the corresponding offset when the ray travels from the source to the edge of the Fresnel zone with certain traveltime t_F. The geometry for calculating the radius of Fresnel zone in a homogeneous ISO and VTI model is shown in Fig. 3.

In order to obtain an analytic expression in VTI model, we define the perturbation series for Fresnel radius squared up to third order by

$$X_F^2 = M_0 + M_1\eta + M_2\eta^2 + M_3\eta^3. \tag{6}$$

For the elliptical case ($\eta = 0$), the traveltime and offset squared are shown by

$$X^2(p)_{\eta=0} = \frac{p_F^2t_0^2V_n^4}{1-p_F^2V_n^2},$$
$$T^2(p)_{\eta=0} = \frac{t_0^2}{1-p_F^2V_n^2}, \tag{7}$$

where the slowness for the elliptical assumption is given by

$$p_F = \frac{\sqrt{t_F^2-t_0^2}}{t_FV_n}. \tag{8}$$

The zeroth-order coefficient M_0 is computed by

$$M_0 = X^2(p)_{\eta=0} = \frac{p_F^2t_0^2V_n^4}{1-p_F^2V_n^2} = \left(t_F^2-t_0^2\right)V_n^2. \tag{9}$$

The other coefficients (see Appendix A) in eq. (6) are given by

$$M_1 = \frac{2\left(t_F^2-t_0^2\right)^2V_n^2}{t_F^2},$$
$$M_2 = \frac{4t_0^2\left(t_F^2-t_0^2\right)^3V_n^2}{t_F^6},$$
$$M_3 = \frac{24t_0^4\left(t_F^2-t_0^2\right)^4V_n^2}{t_F^{10}}. \tag{10}$$

In order to stabilize the approximation and improve the accuracy, two types of Shanks transform (Bender & Orszag 1978) are defined on the perturbation series in eq. (6) given by

$$X_{S1}^2 = \frac{X_0X_2-X_1^2}{X_0+X_2-2X_1},$$
$$X_{S2}^2 = \frac{X_1X_3-X_2^2}{X_1+X_3-2X_2}, \tag{11}$$

where $X_k^2 = \sum_{j=0}^{k} M_j\eta^j$, $k = 0, 1, 2, 3$. The perturbation coefficients M_j ($j = 0, 1, 2, 3$) are given in eqs (9) and (10).

In order to test the accuracy of the approximations above, we introduce a VTI model with the parameters: $V_0 = 2\,\mathrm{km\,s^{-1}}$, $V_n = 2.2\,\mathrm{km\,s^{-1}}$ and $\eta = 0.2$, and plot the relative error in Fresnel radius versus corresponding traveltime (t_F), depth and frequency by using the approximations from second and third perturbation series and the Shanks transforms in Fig. 4. Note that the Fresnel zone varies with depth at frequency $f = 30\,\mathrm{Hz}$ and the Fresnel zone varies with frequency at depth $z = 2\,\mathrm{km}$. One can see that the accuracy from third order perturbation series is higher than second order and the Shanks transform improves the accuracy greatly for both second and third order series. The second order Shanks transform approximation X_{S2} results in the most accurate result and even as accurate as the exact one. We plot the Fresnel zone radius approximation X_{S2} versus anisotropic parameters δ (with $\eta = 0.2$) and η (with $\delta = 0.1$) in Fig. 5. One can see that the Fresnel radius is increasing both with δ and η, and it is more sensitive with δ. The radius of Fresnel zone using the approximation X_{S2} in ISO and VTI models versus traveltime t_F, depth and frequency are shown in Fig. 6. The tendency for the Fresnel zone radius with respect to traveltime, depth and frequency for ISO and VTI models is very similar. We plot the shape of Fresnel zone for ISO ($V = 2\,\mathrm{km\,s^{-1}}$, $f = 30\,\mathrm{Hz}$ and $z = 2\,\mathrm{km}$) and VTI ($V_0 = 2\,\mathrm{km\,s^{-1}}$, $V_n = 2.2\,\mathrm{km\,s^{-1}}$, $\eta = 0.2$, $f = 30\,\mathrm{Hz}$ and $z = 2\,\mathrm{km}$) models in Fig. 7. One can see that, similar to ISO case, the Fresnel zone in VTI model is also a circle but with a larger radius as the velocity in VTI model is independent with the azimuth. Note that the exact numerical results or the reference results are obtained from performing the dynamic ray tracing on the parametric offset-traveltime in eq. (5). Similar to the moveout approximation $t(x)$, the Fresnel zone radius using the traveltime parameters can be treated as $x(t)$. The exact results can be computed from the parametric offset-traveltime equation shown in eq. (5).

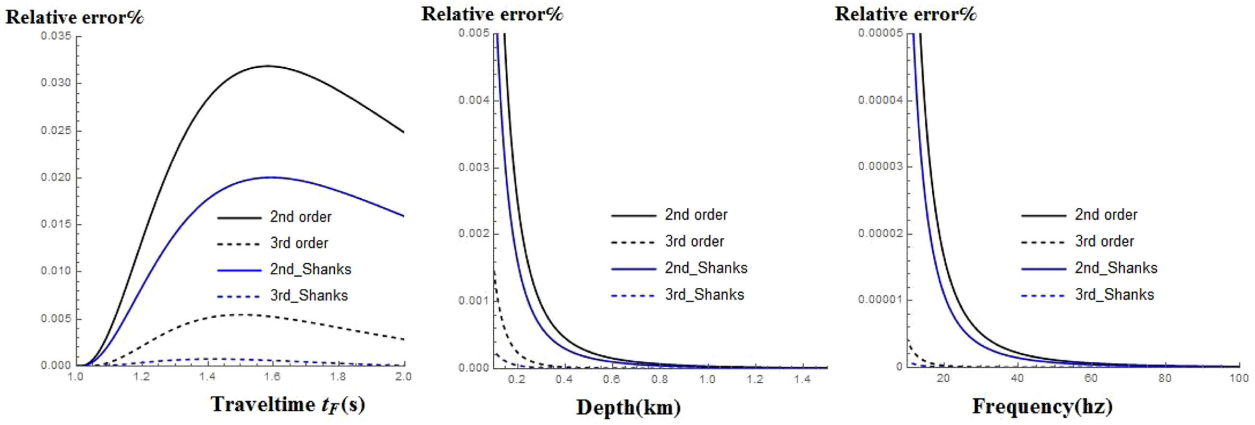

Figure 4. The relative error in Fresnel radius versus the corresponding traveltime (left), depth (middle) and frequency (right) using four types of approximation in VTI model. (Note that the Fresnel zone varies with depth at frequency $f = 30$ Hz and the Fresnel zone varies with frequency at depth $z = 2$ km.)

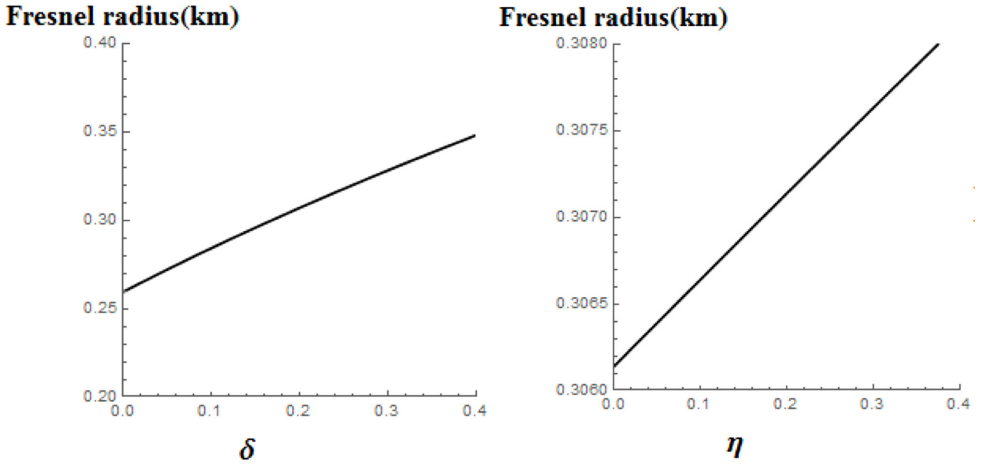

Figure 5. The Fresnel radius using second order Shanks transform approximation X_{S2} versus anisotropy parameters δ (with $\eta = 0.2$) and η (with $\delta = 0.1$).

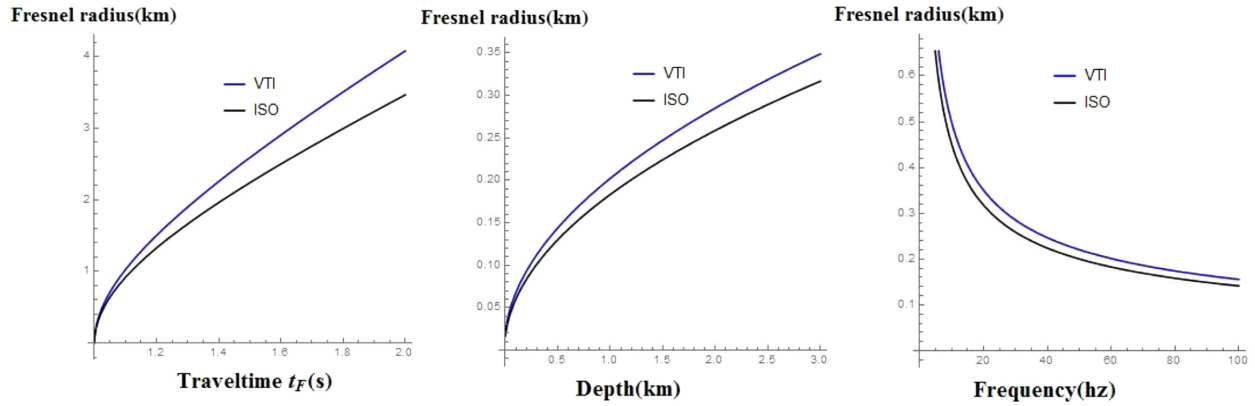

Figure 6. The radius of Fresnel zone in ISO and VTI models versus traveltime (left), depth (middle) and frequency (right). The Fresnel radius computed from ISO and VTI models is shown by black and blue colours, respectively. (Note that the Fresnel zone varies with depth at frequency $f = 30$ Hz; The Fresnel zone varies with frequency at depth $z = 2$ km.)

THE FRESNEL ZONE IN AN ORT MEDIUM

To compute the azimuth-dependent radius of the Fresnel zone for a homogeneous ORT model, we use exact parametric offset and traveltime equations (Stovas 2015):

$$x\left(p_x, p_y\right) = p_x F_2^2 \frac{V_{n1}^2 t_0}{f_1^{1/2} f_2^{3/2}},$$

$$y\left(p_x, p_y\right) = p_y F_1^2 \frac{V_{n2}^2 t_0}{f_1^{1/2} f_2^{3/2}},$$

$$t\left(p_x, p_y\right) = \frac{t_0\left(F_1^2 p_y^2 V_{n2}^2 + F_2^2 p_x^2 V_{n1}^2 + f_1 f_2\right)}{f_1^{1/2} f_2^{3/2}}, \tag{12}$$

where x and y are the corresponding offset projections, and

$$F_1 = 1 - p_x^2 V_{n1}^2 \left(2\eta_1 - \eta_{xy}\right),$$

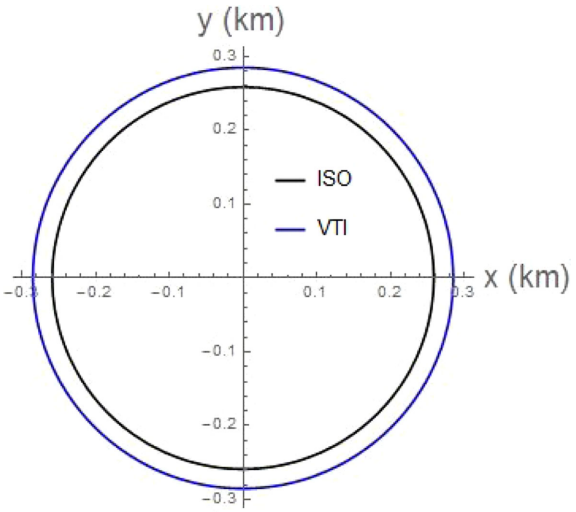

Figure 7. The Fresnel zone in ISO and VTI models. The Fresnel zone computed from ISO and VTI models is shown by black and blue colours, respectively.

$$
\begin{aligned}
F_2 &= 1 - p_y^2 V_{n2}^2 \left(2\eta_2 - \eta_{xy}\right), \\
f_1 &= 1 - (1+2\eta_1)\, p_x^2 V_{n1}^2 - (1+2\eta_2)\, p_y^2 V_{n2}^2 \\
&\quad + \left((1+2\eta_1)(1+2\eta_2) - \left(1+\eta_{xy}\right)^2\right) p_x^2 p_y^2 V_{n1}^2 V_{n2}^2, \\
f_2 &= 1 - 2\eta_1 p_x^2 V_{n1}^2 - 2\eta_2 p_y^2 V_{n2}^2 + \left(4\eta_1\eta_2 - \eta_{xy}^2\right) p_x^2 p_y^2 V_{n1}^2 V_{n2}^2,
\end{aligned}
\tag{13}
$$

with V_0, V_{n1}, V_{n2} being the vertical and NMO velocities. NMO velocities V_{n1} and V_{n2} are defined in $[X, Z]$ and $[Y, Z]$ planes, respectively. Anellipticity parameters η_1 and η_2 are defined in corresponding two vertical symmetry $[X, Z]$ and $[Y, Z]$ planes. The cross-term anellipticity parameter η_{xy} is defined as (Stovas 2015)

$$
\eta_{xy} = \sqrt{\frac{(1+2\eta_1)(1+2\eta_2)}{1+2\eta_3}} - 1, \tag{14}
$$

where anellipticity parameter η_3 is defined in the $[X, Y]$ plane (Vasconcelos & Tsvankin 2006).

Similar to VTI case, by setting the traveltime t equal to t_F, we relate the Fresnel zone $R(X_F, Y_F)$ with the depth of reflector. We introduce a homogeneous ORT model with parameters: $V_0 = 2\,\mathrm{km\,s^{-1}}$, $V_{n1} = 2.2\,\mathrm{km\,s^{-1}}$, $V_{n2} = 2.4\,\mathrm{km\,s^{-1}}$, $\eta_1 = 0.2$, $\eta_2 = 0.15$, $\eta_{xy} = 0.2$, $f = 30\,\mathrm{Hz}$ and the depth of the horizontal reflector is $z = 2\,\mathrm{km}$ and show the exact Fresnel zone $R(X_F, Y_F)$ for ORT model with a quasi-elliptic shape in Fig. 8. Note that similar to the VTI case, the exact solution is computed from performing the dynamic ray tracing in the parametric offsets-traveltime equaiton through the ray parameters (two horizontal slownesses) shown in eq. (12).

In order to get the analytic expression of the azimuth-dependent radius for the Fresnel zone in ORT model, we define the perturbation series up to the second order by

$$
R_F^2 = x_F^2 + y_F^2 = N_0 + \sum_{j=1,2,3} N_j \eta_j + \sum_{i,j=1,2,3} N_{ij} \eta_i \eta_j, \tag{15}
$$

where $3 \equiv xy$, the perturbation coefficients N_j and N_{ij} are given by the model parameters: V_0, V_{n1}, V_{n2}, η_1, η_2, η_{xy}, the frequency f and the group azimuth Φ. To compute the perturbation coefficients, we format the parametric offset and traveltime squared from two projections into the radial offset and the azimuth given by Koren & Ravve (2014)

$$
\begin{aligned}
R^2(p_r, \phi) &= x^2(p_r, \phi) + y^2(p_r, \phi), \\
T^2(p_r, \phi) &= t^2(p_r, \phi),
\end{aligned}
\tag{16}
$$

with the relations

$$
\begin{aligned}
p_x &= p_r \cos(\phi), \\
p_y &= p_r \sin(\phi).
\end{aligned}
\tag{17}
$$

Angle ϕ in eq. (16) is the phase azimuth. The group azimuth Φ can be computed from the following transform in the ellipsoidal assumption (Stovas 2015),

$$
\tan(\Phi) = \frac{V_{n2}^2}{V_{n1}^2} \tan(\phi). \tag{18}
$$

Note that this equation is correct not only for the ellipsoidal assumption, but also as zero-order approximation for any non-elliptic VTI media with arbitrarily large intrinsic anellipticity η, but for infinitesimal (actually, close to zero) offset or horizontal slowness. Otherwise, the transform between the acquisition azimuth and the phase azimuth will include, in addition to this zero-order term, also other terms with (even) powers of offset or horizontal slowness.

The analytic expression for Fresnel zone in ORT model in eq. (15) is derived by equating the exact eq. (12) by setting the traveltime into t_F with the perturbation series defined in eq. (15).

The coefficient N_0 is computed by setting all anellipticity parameters into zero given by

$$
N_0 = \left(t_F^2 - t_0^2\right) V_n^2(\Phi), \tag{19}
$$

where $V_n(\Phi)$ is the NMO ellipse (Grechka & Tsvankin 1999) with

$$
\frac{1}{V_n^2(\Phi)} = \frac{\cos(\Phi)^2}{V_{n1}^2} + \frac{\sin(\Phi)^2}{V_{n2}^2}. \tag{20}
$$

The coefficient N_0 provides the radius squared of Fresnel zone in the ellipsoidal isotropic medium. The other perturbation coefficients N_j and N_{ij} are computed by equating the exact expressions with the perturbation series shown in Appendix B.

Using the ORT model above, we show the polar plots of sensitivity computed from first order (left), quadratic (middle) and cross-term (right) coefficients in the perturbation series versus the group azimuth in Fig. 9, respectively. One can see from the plots that for

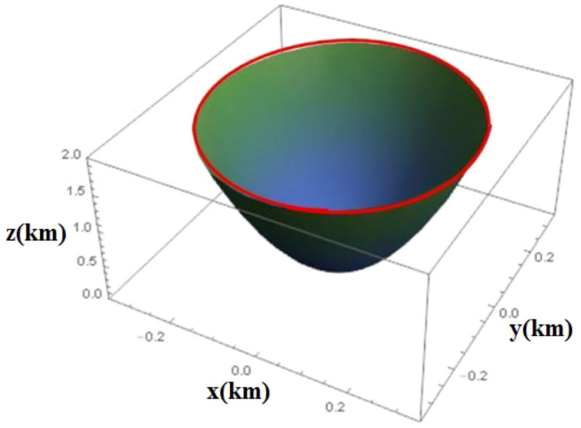

Figure 8. The Fresnel zone computed for a homogeneous ORT model. The model parameters are: $V_0 = 2\,\mathrm{km\,s^{-1}}$, $V_{n1} = 2.2\,\mathrm{km\,s^{-1}}$, $V_{n2} = 2.4\,\mathrm{km\,s^{-1}}$, $\eta_1 = 0.2$, $\eta_2 = 0.15$, $\eta_{xy} = 0.2$ and $f = 30\,\mathrm{Hz}$. The depth of the horizontal reflector is $z = 2\,\mathrm{km}$. The Fresnel zone in ORT model has a quasi-elliptical shape.

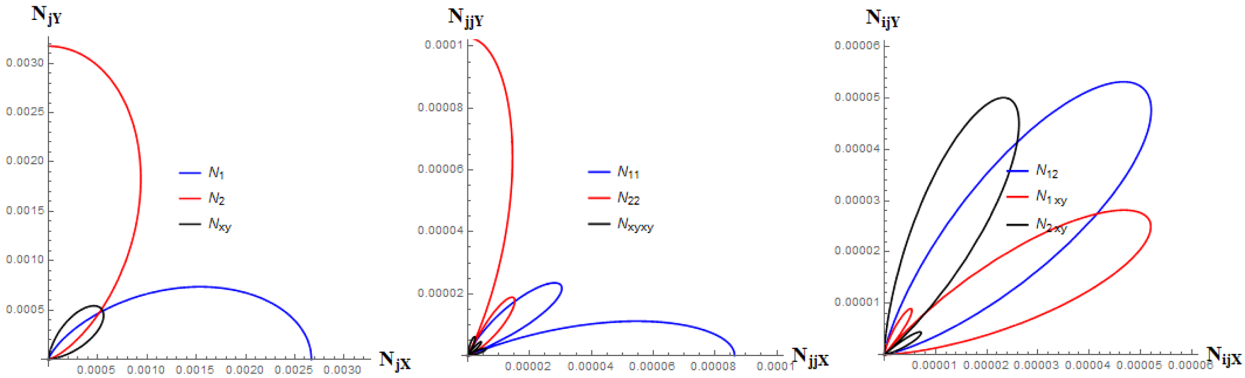

Figure 9. The sensitivity computed from first order (left), quadratic (middle) and cross-term coefficients in eq. (15) in the perturbation series for Fresnel zone versus the group azimuth. The depth of the horizontal reflector is $z = 2$ km.

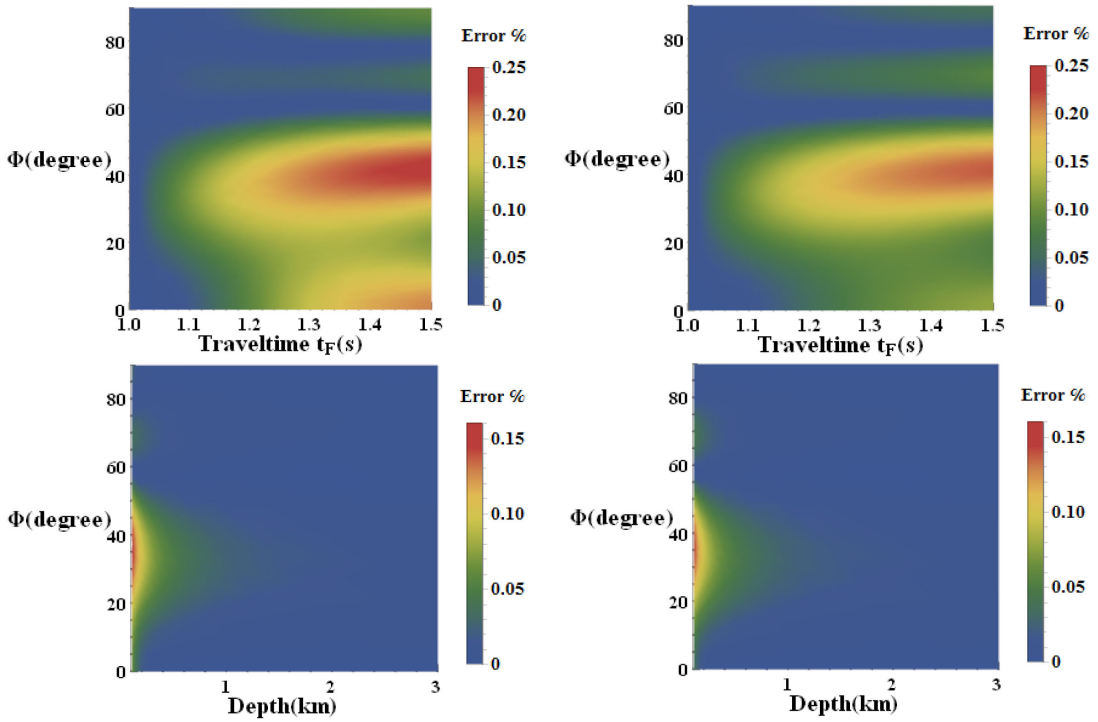

Figure 10. The contour plot of error in R_F from two approximations for ORT model plotted versus corresponding traveltime and the group azimuth (top) and depth and the group azimuth (bottom). The perturbation series approximation and Shanks transform are shown in left and right, respectively. The model parameters are given in caption for Fig. 8.

first and quadratic order coefficients, the sensitivity in anellipticity parameters η_1 and η_2 have the similar shapes and reach the maximal values for 0 and $\pi/2$ azimuth angle, respectively. The sensitivity in cross-term anellipticity parameter η_{xy} reaches its maximal value at $\pi/4$ azimuth angle for first order coefficient. For quadratic order coefficient, the sensitivity to cross-term anellipticity parameter is very small. For cross-term coefficients, the sensitivity to anellipticity parameters $\eta_1\eta_2$ reaches the maximal value at $\pi/4$ azimuth angle. For the sensitivity to anellipticity parameters $\eta_1\eta_{xy}$ and $\eta_2\eta_{xy}$, they obtain their maximal values at around $\pi/6$ and $\pi/3$ azimuth angle, respectively.

Similar to the approximations in VTI case, the Shanks transform can also be applied to the perturbation series in ORT model (eq. 15) and results in

$$R_S = N_0 + \frac{R_1^2}{R_1 - R_2}, \tag{21}$$

where N_0 is defined in eq. (19), $R_1 = \sum_i N_i\eta_i$ and $R_2 = \sum_{ij} N_{ij}\eta_i\eta_j$, $(i, j = 1, 2, xy)$ are the first- and second-order term coefficients are given in Appendix B (eqs B10, B12 and B14).

NUMERICAL EXAMPLES

In order to test the accuracy of the Fresnel zone approximation in ORT model, we use the ORT model introduced above with the parameters: $V_0 = 2\,\mathrm{km\,s^{-1}}$, $V_{n1} = 2.2\,\mathrm{km\,s^{-1}}$, $V_{n2} = 2.4\,\mathrm{km\,s^{-1}}$, $\eta_1 = 0.2$, $\eta_2 = 0.15$ and $\eta_{xy} = 0.2$. Note that for the computation versus traveltime $t_0 = 1\,rms$, the computation versus depth $f = 30$ Hz and the computation versus frequency $z = 2$ km. The relative error in Fresnel zone with two approximations (perturbation series and the Shanks transform) using the ORT model above versus corresponding (traveltime, group azimuth) and (depth, group azimuth) is shown in Fig. 10, respectively. One can see that for the error plotted with traveltime t_F, the maximal error is obtained at

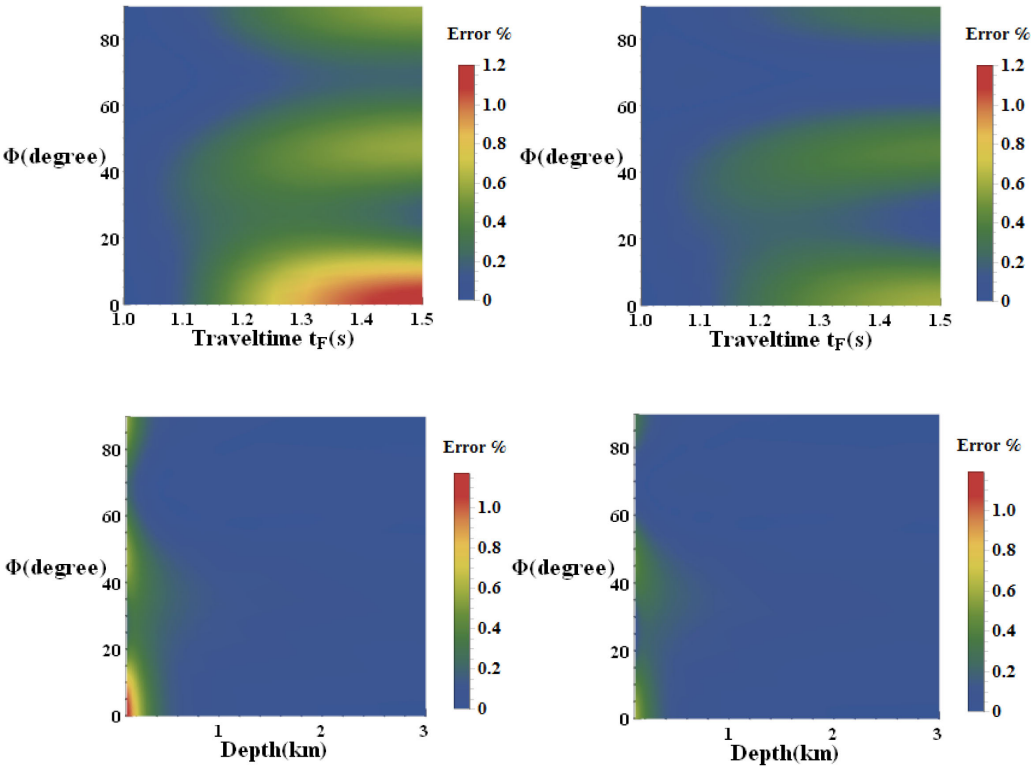

Figure 11. The contour plot of error in R_F from two approximations for ORT model plotted versus corresponding traveltime and the group azimuth (top) and depth and the group azimuth (bottom). The perturbation series approximation and Shanks transform are shown in left and right, respectively. The ORT model parameters are defined with the velocities specified in the caption for Fig. 8 and the higher anellipticity parameters: $\eta_1 = 0.4$, $\eta_2 = 0.3$ and $\eta_{xy} = 0.4$.

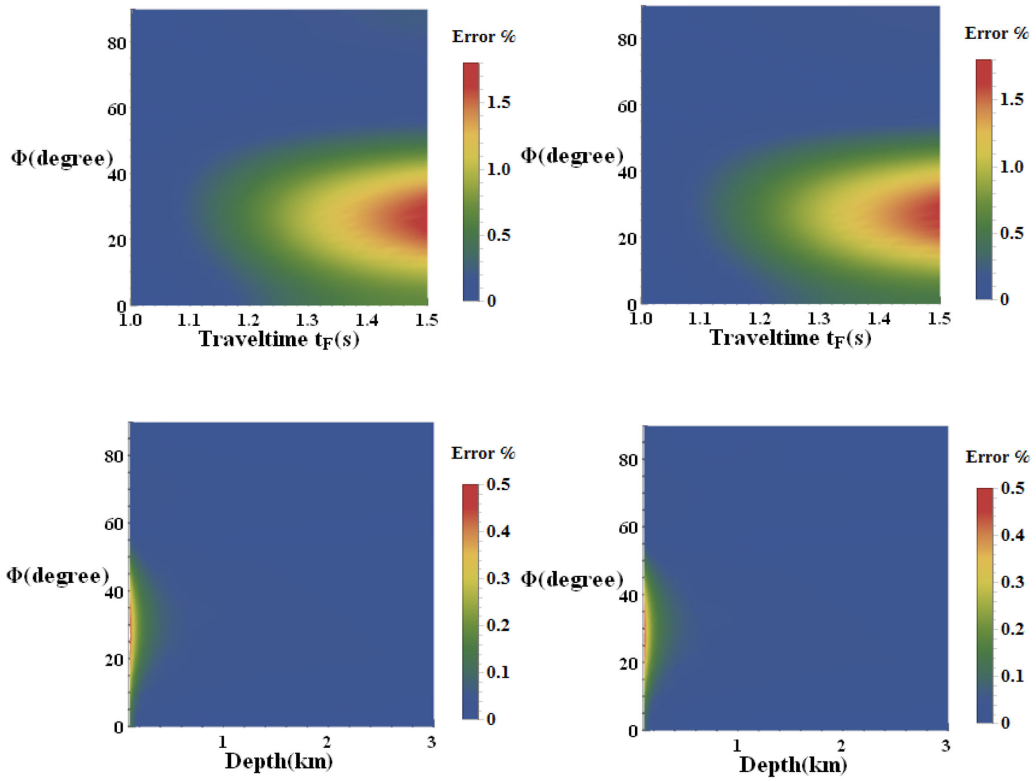

Figure 12. The contour plot of error in R_F from two approximations for ORT model plotted versus corresponding traveltime and the group azimuth (top) and depth and the group azimuth (bottom). The perturbation series approximation and Shanks transform are shown in left and right, respectively. The ORT model parameters are defined with the velocities specified in the caption for Fig. 8 and the negative anellipticity parameters: $\eta_1 = -0.2$, $\eta_2 = -0.15$ and $\eta_{xy} = -0.2$.

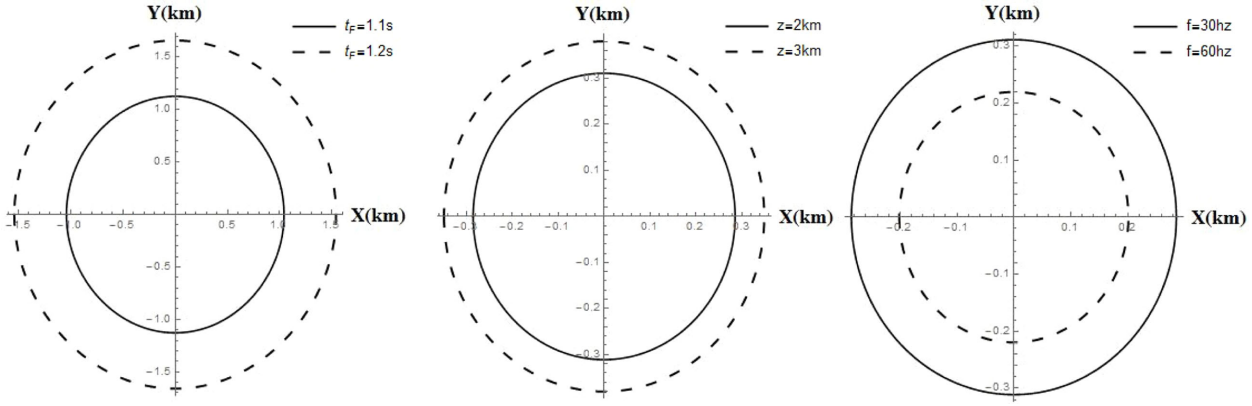

Figure 13. The Fresnel zone computed for ORT model for different traveltime (left), depth (middle) and frequency (right) using the ORT model with parameters given in the caption for Fig. 8.

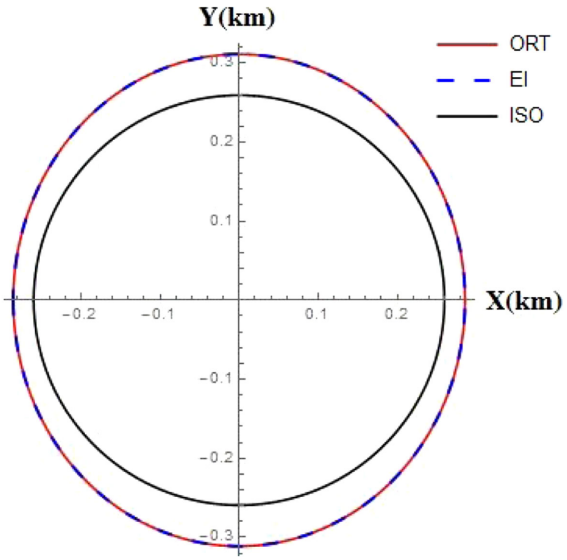

Figure 14. The shape of the Fresnel zone computed for ISO, EI and ORT models. The depth of the horizontal reflector is $z = 2$ km.

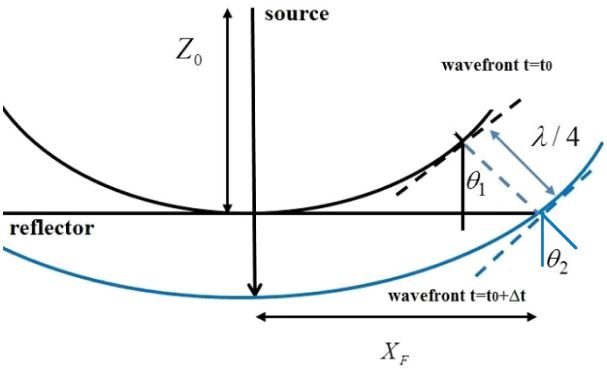

Figure 15. The diagram showing the Fresnel zone in an anisotropic medium. Angles θ_1 and θ_2 are phase angles measured in corresponding points at wave fronts $t = t_0$ and $t = t_0 + \Delta t$, respectively.

about 40° azimuth for traveltime $t_F = 1.5$ s, for the plots versus depth, the maximal error is obtained at zero depth around 35° azimuth for two approximations and the accuracy from these two approximations is almost the same. The Shanks transform does not help a lot in improving the accuracy on the perturbation series for the Fresnel zone radius approximation, the reason for this is that the sensitivity in perturbation coefficients is very small (shown in Fig. 9), the effect by using the Shanks transform is not obvious. We show another numerical example with higher anellipticity parameters with $\eta_1 = 0.4$, $\eta_2 = 0.3$ and $\eta_{xy} = 0.4$, while keeping the remaining model parameters the same in Fig. 11. Compared with the plots in Fig. 10, the error for the ORT model with higher anellipticity parameters is larger and the effect from the Shanks transform is more significant. One more numerical example, with all negative anellipticity parameters: $\eta_1 = -0.2$, $\eta_2 = -0.15$ and $\eta_{xy} = -0.2$, while keeping the same remaining model parameters, is shown in Fig. 12. One can tell that comparing with the plots in Fig. 10 the error from negative anellipticity parameters is larger. Similar to the plots in Fig. 10, the effect from the Shanks transform is not obvious.

Using the Shanks transform approximation in eq. (21), we show the radius of the Fresnel zone versus different traveltime, depth and frequency in Fig. 13. One can see from the plots that the radius increases with traveltime and depth while decreases with frequency.

Selecting a horizontal reflector with the depth $z = 2$ km, we show the shape of the Fresnel zone using the Shanks transform approximation (shown in eq. 21) for ORT, elliptical isotropic (EI), and ISO model in Fig. 14, respectively. Note that for EI model, all anellipticity parameters are zero ($\eta_1 = \eta_2 = \eta_3 = 0$), for ISO model, there is one velocity with $V = V_0 = V_{n1} = V_{n2} = 2\,\mathrm{km\,s^{-1}}$. One can see from the plots that the Fresnel zones for ORT and EI model almost coincide that indicates that less sensitivity of the Fresnel zone in anellipticity parameters, which is also explained by the polar plots in Fig. 9. For ISO case, the Fresnel zone is just a circle with the radius smaller than the ones in ORT and EI model.

Note that the advantage of this paper is an attempt of a direct offset-traveltime approximation, perturbing the anellipticity of VTI, or the three anellipticities of ORT medium. The Fresnel zone calculation is a particular case for this method, when the time is the Fresnel zone traveltime, and the offset is its radius. Similarly, the moveout approximation can also be derived from the same strategy.

DISCUSSIONS

The reason why we derive the approximation for the Fresnel zone using the traveltime is to avoid the complexity in dealing with the phase domain velocities. By the definition, the Fresnel zone radius is defined by the lateral projection when the seismic wave propagates for 1/4 wavelength after arriving the reflector with $\lambda = \frac{V_\theta}{f}$, V_θ is

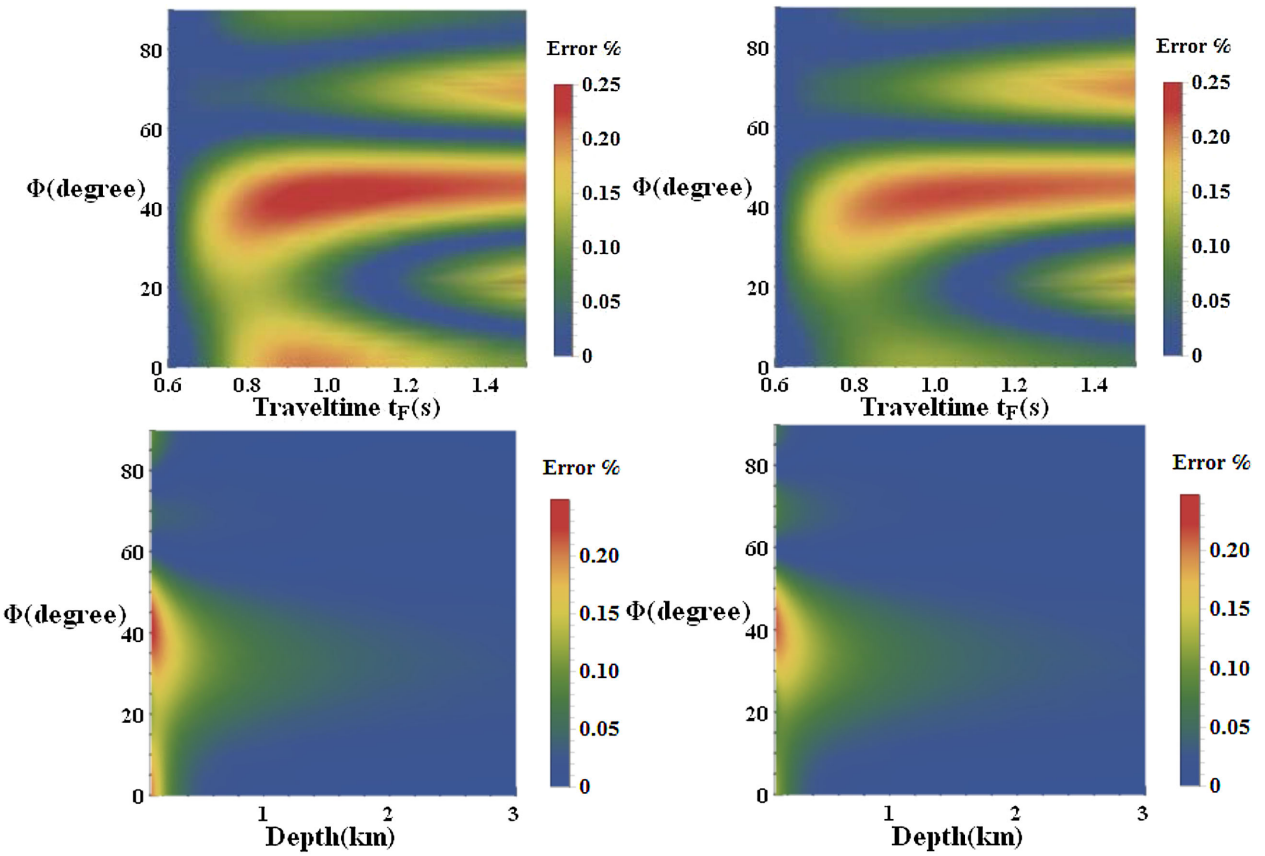

Figure 16. The contour plot of error in R_F from two approximations for ORT model plotted versus corresponding traveltime and the group azimuth (top) and depth and the group azimuth (bottom). The perturbation series approximation and Shanks transform are shown in left and right, respectively. The ORT model parameters are: top—$t_0 = 0.6$ s, $V_{n1} = 2.2\,\mathrm{km\,s^{-1}}$, $V_{n2} = 2.4\,\mathrm{km\,s^{-1}}$, $\eta_1 = 0.2$, $\eta_2 = 0.15$ and $\eta_{xy} = 0.2$; bottom—$V_0 = 2\,\mathrm{km\,s^{-1}}$, $V_{n1} = 2.2\,\mathrm{km\,s^{-1}}$, $V_{n2} = 2.4\,\mathrm{km\,s^{-1}}$, $\eta_1 = 0.2$, $\eta_2 = 0.15$, $\eta_{xy} = 0.2$ and $f = 10$ Hz.

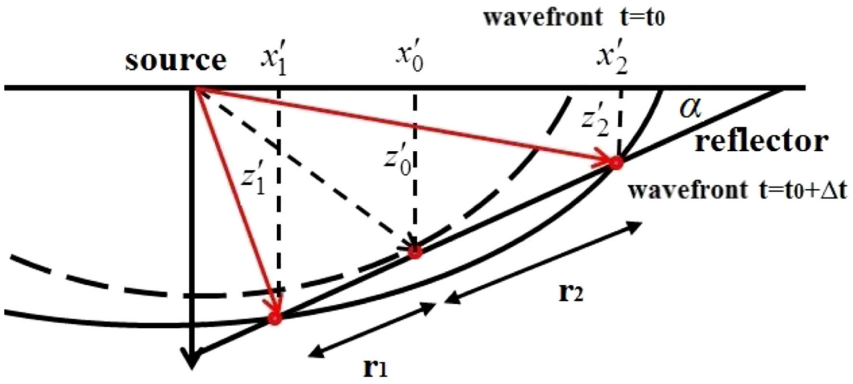

Figure 17. The sketch showing the Fresnel zone for a dip reflector in a homogeneous VTI model.

the wave-front velocity (phase velocity) with the phase angle θ. Shown in Fig. 15, if the model is isotropic, the phase angle θ_1 measured at wave front ($t = t_0$) is equal to θ_2 measured at wave front ($t = t_0 + \Delta t$). However, for the anisotropic model, two wave fronts are not parallel ($\theta_1 \neq \theta_2$), to compute the Fresnel zone radius X_F, the change in the phase angle needs to be taken into consideration, which makes the computation much more complicated. Using the traveltime parameters, what we are interested in is the ray traveling from the source to the reflector with the certain traveltime $t_F = t_0 + \Delta t$ (Fig. 1, bottom) that makes the derivation much simpler for anisotropic media.

In order to singularize the anomaly of error plot in ORT model, we apply one more numerical example from the perturbation series (eq. 15) and the Shanks transform approximation (eq. 21) in Fig. 16, (left and right, respectively) with a smaller t_0 ($t_0 = 0.6$ s) and frequency ($f = 10$ Hz). One can see that for the error plot versus traveltime and group azimuth, the shape of the anomaly is more obvious and maximal error is obtained at the centre of the anomaly. For the error plot versus depth and group azimuth, the maximal error is obtained at about 40° azimuth when the depth is zero.

This perturbation based method for the Fresnel zone in the anisotropic model can be extended for the model with a dip

reflector. Shown in Fig. 17, the Fresnel zone for a dip reflector with the dip angle α in a homogenous VTI model is consist of two parts (r_1 and r_2), which is the corresponding distance in two directions along the dip reflector when the seismic wave propagates within 1/4 wavelength after it first touches the dip reflector. We assume the value of the dip angle α and the depth of the first touching point z_0' are known. The Fresnel zones (r_1 and r_2) are calculated by

$$r_1 = \frac{x_0' - x_1'}{\cos\alpha}, \quad r_2 = \frac{x_2' - x_0'}{\cos\alpha}, \tag{22}$$

where x_0' is the offset for the first touching point, x_1' and x_2' are the corresponding offsets for the Fresnel zone boundary point with the corresponding depth z_1' and z_2'. The corresponding offsets x_1' and x_2' are computed by the Shanks transform approximation shown in eq. (10) with the certain traveltime $t_F = t_0 + \Delta t$

$$\begin{aligned} x_1' &= \left\{z_1', t_F, V_0, V_n, \eta, \alpha\right\}, \\ x_2' &= \left\{z_2', t_F, V_0, V_n, \eta, \alpha\right\}, \end{aligned} \tag{23}$$

where the two corresponding depth z_1' and z_2' are obtained from the Pythagorean theorem

$$\begin{aligned} \frac{z_0'}{\tan\alpha} + \left(x_0' - x_1'\left[z_1'\right]\right) &= z_1' \tan\alpha \Rightarrow z_1', \\ \frac{z_0'}{\tan\alpha} - \left(x_2'\left[z_2'\right] - x_0'\right) &= z_2' \tan\alpha \Rightarrow z_2'. \end{aligned} \tag{24}$$

Note that on contrary to the horizontal reflector case, the Fresnel zone is not symmetric for dip reflector case ($r_1 \neq r_2$).

CONCLUSIONS

We derive the form of Fresnel zone radius using the traveltime parameter and use it to obtain the analytic expressions in an acoustic VTI and ORT models from the exact offset-traveltime parametric equation using the perturbation method. The analysis of the Fresnel zone radius is applied versus corresponding traveltime, depth and the frequency. One can tell that the Fresnel zone radius in anisotropic media (VTI and ORT) increases with traveltime and depth, while decreases with frequency. The Shanks transform is applied to stabilize the approximation and improve the accuracy for both two models. Shown from the numerical examples that for VTI model, the second order Shanks transform is the most accurate approximation that is almost as accurate as the exact one. For ORT model, the quasi-elliptical shape is obtained for the Fresnel zone. The perturbation series and the Shanks transform approximation are all very accurate and almost the same accuracy for the Fresnel zone calculation due to the small sensitivity in perturbation coefficients.

ACKNOWLEDGEMENTS

We would like to acknowledge China Scholarship Council (CSC) and ROSE project for financial support. We also acknowledge I. Ravve and an anonymous reviewer for their valuable comments.

REFERENCES

Alkhalifah, T., 1998. Acoustic approximations for processing in transversely isotropic media, *Geophysics,* **63,** 623–631.
Alkhalifah, T. & Tsvankin, I., 1995. Velocity analysis for transversely isotropic media, *Geophysics,* **60,** 1550–1566.
Bender, C.M. & Orszag, S.A., 1978. *Advanced Mathematical Methods for Scientists and Engineers,* McGraw-Hill.
Červený, V., 2001. *Seismic Ray Theory, Cambridge Univ*. Press.
Červený, V. & Soares, J., 1992. Fresnel volume ray tracing, *Geophysics,* **57,** 902–915.
Eaton, D.W., Stewart, R.R. & Harrison, M.P., 1991. The Fresnel zone for *P–SV* waves, *Geophysics,* **56,** 360–364.
Favretto-Cristini, N., Cristini, P. & deBazelaire, E., 2007a. Influence of the interface Fresnel zone on the reflected *P*-wave amplitude modelling, *Geophys. J. Int.,* **171,** 841–846.
Favretto-Cristini, N., Cristini, P. & deBazelaire, E., 2007b. Some reflections on reflectors and wave amplitudes, *Acta Acust. united with Acust.,* **93,** 909–916.
Grechka, V. & Tsvankin, I., 1999. 3-D moveout velocity analysis and parameter estimation for orthorhombic media, *Geophysics,* **64,** 820–837.
Hagedoorn, J.G., 1954. A process of seismic reflection interpretation, *Geophys. Prospect.,* **2,** 85–127.
Hristov, H.D., 2000. *Fresnal Zones in Wireless Links, Zone Plate Lenses and Antennas,* Artech House, Inc.
Hubral, P., Schleicher, J., Tygel, M. & Hanitzch, Ch., 1993. Determination of Fresnel zones from traveltime measurements, *Geophysics,* **58,** 703–712.
Koren, Z. & Ravve, I., 2014. Azimuthally dependent anisotropic velocity model update, *Geophysics,* **79,** C27–C53.
Lindsey, J.P., 1989. The Fresnel zone and its interpetive significance, *Leading Edge,* **7,** 33–39.
Monk, D., 2009. Fresnel zone binning: application to 3D seismic fold and coverage assessments, *Leading Edge,* **28,** 288–295.
Monk, D., 2010. Fresnel-zone binning: Fresnel-zone shape with offset and velocity function, *Geophysics,* **75,** T9–T14.
Moser, T.J. & Červený, V., 2007. Paraxial ray methods for anisotropic inhomogeneous media, *Geophys. Prospect.,* **55,** 21–37.
Okoye, P. & Uren, N., 2000. Fresnel zones and spatial resolution for *P*- and *SH*-waves in transversely isotropic media, *Geophysics,* **65,** 1168–1178.
Schleicher, J., Hubral, P., Jaya, M. & Tygel, M., 1997. Minimum apertures and Fresnel zones in migration and demigration, *Geophysics,* **62,** 183–194.
Sheriff, R.E., 1980. Nomogram for Fresnel-zone calculation, *Geophysics,* **45,** 968–972.
Sheriff, R.E., 1996. Understanding the Fresnel zone, *AAPG Explorer,* 18–19
Spetzler, J. & Snieder, R., 2004. The Fresnel volume and transmitted waves, *Geophysics,* **69,** 653–663.
Stovas, A., 2015. Azimuthally dependent kinematic properties of orthorhombic media, *Geophysics,* **80,** C107–C122.
Thomsen, L., 1986. Weak elastic anisotropy, *Geophysics,* **51,** 1954–1966.
Trorey, A.W., 1970. A simple theory for seismic diffractions, *Geophysics,* **35,** 762–784.
Ursin, B., Favretto-Cristini, N. & Cristini, P., 2014. Fresnel volume and interface Fresnel zone for reflected and transmitted waves from a curved interface in anisotropic media, *Geophysics,* **79,** C123–C134.
Vasconcelos, I. & Tsvankin, I., 2006. Non-hyperbolic moveout inversion of wide-azimuth *P*-wave data for orthorhombic media, *Geophys. Prospect.,* **54,** 535–552.
Widess, M.B., 1982. Quantifying resolving power of seismic systems, *Geophysics,* **47,** 1160–1173.

APPENDIX A: THE ANALYTIC EXPRESSION FOR FRESNEL ZONE IN A HOMOGENEOUS VTI MODEL USING THE PERTURBATION METHOD

In order to obtain an analytic expression for Fresnel radius squared in VTI model, we define the perturbation series up to third order by

$$X_F^2 = M_0 + M_1\eta + M_2\eta^2 + M_3\eta^3. \tag{A1}$$

For elliptical case ($\eta = 0$), the traveltime and offset squared are obtained from the parametric equation (5) by

$$\begin{aligned} X^2(p)_{\eta=0} &= \frac{p_F^2 t_0^2 V_n^4}{1 - p_F^2 V_n^2}, \\ T^2(p)_{\eta=0} &= \frac{t_0^2}{1 - p_F^2 V_n^2}, \end{aligned} \tag{A2}$$

where $p_F = \frac{\sqrt{t_F^2 - t_0^2}}{t_F V_n}$ for the elliptical assumption. The zeroth-order coefficient M_0 is computed by

$$M_0 = X^2(p)_{\eta=0} = \frac{p_F^2 t_0^2 V_n^4}{1 - p_F^2 V_n^2} = \left(t_F^2 - t_0^2\right) V_n^2. \tag{A3}$$

The first-order coefficient is obtained by

$$M_1 = \left[\frac{\partial X^2(p)}{\partial \eta} - \frac{\partial M_0\left(t_F^2 \to t^2\right)}{\partial \eta}\right] = \frac{2\left(t_F^2 - t_0^2\right)^2 V_n^2}{t_F^2}. \tag{A4}$$

Subsequently, we compute the second- and third-order coefficients, given by

$$\begin{aligned} M_2 &= \left[\frac{\partial^2 X^2(p)}{\partial \eta^2} - \frac{\partial M_1\left(t_F^2 \to t^2\right)}{\partial \eta} - \frac{\partial^2 M_0\left(t_F^2 \to t^2\right)}{\partial \eta^2}\right] = \frac{4t_0^2\left(t_F^2 - t_0^2\right)^3 V_n^2}{t_F^6}, \\ M_3 &= \left[\frac{\partial^3 X^2(p)}{\partial \eta^3} - \frac{\partial M_2\left(t_F^2 \to t^2\right)}{\partial \eta} - \frac{\partial^2 M_1\left(t_F^2 \to t^2\right)}{\partial \eta^2} - \frac{\partial^3 M_0\left(t_F^2 \to t^2\right)}{\partial \eta^3}\right] \\ &= \frac{24t_0^4\left(t_F^2 - t_0^2\right)^4 V_n^2}{t_F^{10}}. \end{aligned} \tag{A5}$$

Note that these perturbations coefficients M_i, ($i = 0, ..., 3$) are all η independent since t_F is an argument in the approximation. The parameters for the approximation in VTI model are t_F, t_0 and V_n. The effect for the anellipticity is hidden in parameter t_F. $t_F^2 \to t^2$ means t_F here should use the function form shown in the parametric equation (eq. 5) for derivation after applying the elliptical assumption to get the coefficients (M_1, M_2 and M_3).

APPENDIX B: THE ANALYTIC EXPRESSION FOR FRESNEL ZONE IN A HOMOGENEOUS ORT MODEL USING THE PERTURBATION METHOD

To compute the perturbation coefficients in eq. (15), we format the parametric offset and traveltime squared from two projections into the radius offset and the phase azimuth given by

$$\begin{aligned} R^2(p_r, \phi) &= x^2(p_r, \phi) + y^2(p_r, \phi), \\ T^2(p_r, \phi) &= t^2(p_r, \phi), \end{aligned} \tag{B1}$$

with the relations as below

$$\begin{aligned} p_x &= p_r \cos(\phi), \\ p_y &= p_r \sin(\phi). \end{aligned} \tag{B2}$$

We represent the parametric equations in terms of slowness p_r and the phase azimuth ϕ for the elliptical assumption:

$$\begin{aligned} R^2(p_r, \phi)_{\eta=0} &= \frac{p_r^2 t_0^2\left(V_{n1}^4 \cos(\phi)^2 + V_{n2}^4 \sin(\phi)^2\right)}{1 - p_r^2\left(V_{n1}^2 \cos(\phi)^2 + V_{n2}^2 \sin(\phi)^2\right)}, \\ T^2(p_r, \phi)_{\eta=0} &= \frac{t_0^2}{1 - p_r^2\left(V_{n1}^2 \cos(\phi)^2 + V_{n2}^2 \sin(\phi)^2\right)}, \end{aligned} \tag{B3}$$

which gives

$$p_r = \frac{\sqrt{t_F^2 - t_0^2}}{t_F\sqrt{V_{n1}^2 \cos(\phi)^2 + V_{n2}^2 \sin(\phi)^2}}. \tag{B4}$$

First the coefficient N_0 for the ellipsoidal case is computed by setting all anellipticity parameters into zero given by

$$N_0 = \frac{\left(t_F^2 - t_0^2\right)\left(V_{n1}^4 \cos(\phi)^2 + V_{n2}^4 \sin(\phi)^2\right)}{V_{n1}^2 \sin(\phi)^2 + V_{n2}^2 \cos(\phi)^2}. \tag{B5}$$

Note that the azimuth ϕ in equations above is the phase azimuth. We need to convert the azimuth from phase to group domain by the relation in the elliptic assumption

$$\tan(\Phi) = \frac{V_{n2}^2}{V_{n1}^2}\tan(\phi). \tag{B6}$$

The coefficient N_0 for the ellipsoidal case is terms of group azimuth is given by

$$N_0 = \left(t_F^2 - t_0^2\right) V_n^2(\Phi), \tag{B7}$$

where $V_n(\Phi)$ is the NMO ellipse (Grechka & Tsvankin 1999) with

$$\frac{1}{V_n^2(\Phi)} = \frac{\cos(\Phi)^2}{V_{n1}^2} + \frac{\sin(\Phi)^2}{V_{n2}^2}. \tag{B8}$$

Similar to VTI case, using the perturbation method, we compute the first-order coefficients as following

$$\begin{aligned}
N_1 &= \left[\frac{\partial R_F^2}{\partial \eta_1} - \frac{\partial N_0}{\partial \eta_1}\right]_{\eta_2=\eta_{xy}=0},\\
N_2 &= \left[\frac{\partial R_F^2}{\partial \eta_2} - \frac{\partial N_0}{\partial \eta_2}\right]_{\eta_1=\eta_{xy}=0},\\
N_{xy} &= \left[\frac{\partial R_F^2}{\partial \eta_{xy}} - \frac{\partial N_0}{\partial \eta_{xy}}\right]_{\eta_1=\eta_2=0}.
\end{aligned} \tag{B9}$$

The first-order coefficients N_1, N_2 and N_{xy} in terms of group azimuth are given by

$$\begin{aligned}
N_1 &= \frac{2\cos(\Phi)^4\left(t_F^2 - t_0^2\right)^2 V_{n1}^2 V_{n2}^4\left(V_{n2}^2\cos(\Phi)^2 + \left(4V_{n1}^2 - 3V_{n2}^2\right)\sin(\Phi)^2\right)}{t_F^2\left(V_{n1}^2\sin(\Phi)^2 + V_{n2}^2\cos(\Phi)^2\right)^3},\\
N_2 &= \frac{2\sin(\Phi)^4\left(t_F^2 - t_0^2\right)^2 V_{n1}^4 V_{n2}^2\left(V_{n1}^2\sin(\Phi)^2 + \left(4V_{n2}^2 - 3V_{n1}^2\right)\cos(\Phi)^2\right)}{t_F^2\left(V_{n1}^2\sin(\Phi)^2 + V_{n2}^2\cos(\Phi)^2\right)^3},\\
N_{xy} &= \frac{2\sin(\Phi)^2\cos(\Phi)^2\left(t_F^2 - t_0^2\right)^2 V_{n1}^2 V_{n2}^2\left(2V_{n1}^4\sin(\Phi)^2 - V_{n1}^2 V_{n2}^2 + 2V_{n2}^4\cos(\Phi)^2\right)}{t_F^2\left(V_{n1}^2\sin(\Phi)^2 + V_{n2}^2\cos(\Phi)^2\right)^3}.
\end{aligned} \tag{B10}$$

Subsequently, the quadratic coefficients N_{11}, N_{22} and N_{xyxy} are computed as following

$$\begin{aligned}
N_{11} &= \left[\frac{1}{2}\left(\frac{\partial^2 R_F^2}{\partial \eta_1^2}\right) - \left(\frac{\partial^2 N_0}{\partial \eta_1^2} + \frac{\partial N_1}{\partial \eta_1}\right)\right]_{\eta_2=\eta_{xy}=0},\\
N_{22} &= \left[\frac{1}{2}\left(\frac{\partial^2 R_F^2}{\partial \eta_2^2}\right) - \left(\frac{\partial^2 N_0}{\partial \eta_2^2} + \frac{\partial N_2}{\partial \eta_2}\right)\right]_{\eta_1=\eta_{xy}=0},\\
N_{xyxy} &= \left[\frac{1}{2}\left(\frac{\partial^2 R_F^2}{\partial \eta_{xy}^2}\right) - \left(\frac{\partial^2 N_0}{\partial \eta_{xy}^2} + \frac{\partial N_{xy}}{\partial \eta_{xy}}\right)\right]_{\eta_1=\eta_2=0},
\end{aligned} \tag{B11}$$

and shown in terms of group azimuth by

$$\begin{aligned}
N_{11} &= -\frac{4\cos(\Phi)^6\left(t_F^2 - t_0^2\right)^3 V_{n1}^2 V_{n2}^6}{t_F^6\left(V_{n1}^2\sin(\Phi)^2 + V_{n2}^2\cos(\Phi)^2\right)^5}\left(t_0^2 V_{n2}^4\cos(\Phi)^4 + \left(\left(8t_0^2 + t_F^2\right)V_{n1}^2 - \left(\left(7t_0^2 + 6t_F^2\right)\right)V_{n2}^2\right)V_{n2}^2\sin(\Phi)^2\cos(\Phi)^2\right.\\
&\quad \left. + 5t_F^2 V_{n1}^2\sin(\Phi)^4\left(V_{n2}^2 - 2V_{n1}^2\right)\right),\\
N_{22} &= -\frac{4\sin(\Phi)^6\left(t_F^2 - t_0^2\right)^3 V_{n1}^6 V_{n2}^2}{t_F^6\left(V_{n1}^2\sin(\Phi)^2 + V_{n2}^2\cos(\Phi)^2\right)^5}\left(t_0^2 V_{n1}^4\sin(\Phi)^4 + \left(\left(8t_0^2 + t_F^2\right)V_{n2}^2 - \left(\left(7t_0^2 + 6t_F^2\right)\right)V_{n1}^2\right)V_{n1}^2\sin(\Phi)^2\cos(\Phi)^2\right.\\
&\quad \left. + 5t_F^2 V_{n2}^2\cos(\Phi)^4\left(V_{n1}^2 - 2V_{n2}^2\right)\right),\\
N_{xyxy} &= \frac{\sin(\Phi)^2\cos(\Phi)^2\left(t_F^2 - t_0^2\right)^3 V_{n1}^2 V_{n2}^2}{t_F^6\left(V_{n1}^2\sin(\Phi)^2 + V_{n2}^2\cos(\Phi)^2\right)^5}\left(6t_F^2 V_{n1}^8\sin(\Phi)^6 - V_{n1}^6 V_{n2}^2\left(t_F^2\sin(\Phi)^2 + \left(16t_0^2 + 21t_F^2\right)\cos(\Phi)^2\right)\sin(\Phi)^4\right.,\\
&\quad \left. + 4V_{n1}^4 V_{n2}^4\left(3t_0^2 + 4t_F^2\right)\sin(\Phi)^2\cos(\Phi)^2 - \left(t_F^2\cos(\Phi)^2 + \left(16t_0^2 + 21t_F^2\right)\right)V_{n1}^2 V_{n2}^6\cos(\Phi)^4 + 6t_F^2 V_{n2}^8\cos(\Phi)^6\right).
\end{aligned} \tag{B12}$$

The remaining cross-term coefficients N_{12}, N_{1xy} and N_{2xy} are computed as following

$$
\begin{aligned}
N_{12} &= \left[\frac{\partial^2 R_F^2}{\partial\eta_1\partial\eta_2} - \left(\frac{\partial N_0}{\partial\eta_1}\frac{\partial N_0}{\partial\eta_2} + \frac{\partial N_1}{\partial\eta_2} + \frac{\partial N_2}{\partial\eta_1}\right)\right]_{\eta_{xy}=0},\\
N_{1xy} &= \left[\frac{\partial^2 R_F^2}{\partial\eta_1\partial\eta_{xy}} - \left(\frac{\partial N_0}{\partial\eta_1}\frac{\partial N_0}{\partial\eta_{xy}} + \frac{\partial N_1}{\partial\eta_{xy}} + \frac{\partial N_{xy}}{\partial\eta_1}\right)\right]_{\eta_2=0},\\
N_{2xy} &= \left[\frac{\partial^2 R_F^2}{\partial\eta_2\partial\eta_{xy}} - \left(\frac{\partial N_0}{\partial\eta_2}\frac{\partial N_0}{\partial\eta_{xy}} + \frac{\partial N_2}{\partial\eta_{xy}} + \frac{\partial N_{xy}}{\partial\eta_2}\right)\right]_{\eta_1=0},
\end{aligned}
\tag{B13}
$$

and shown in terms of group azimuth by

$$
\begin{aligned}
N_{12} &= -\frac{8\sin(\Phi)^4\cos(\Phi)^4\left(t_F^2-t_0^2\right)^3 V_{n1}^4 V_{n2}^4}{t_F^6\left(V_{n1}^2\sin(\Phi)^2+V_{n2}^2\cos(\Phi)^2\right)^5}\left(4\left(t_0^2+2t_F^2\right)V_{n1}^4\sin(\Phi)^2 - 3\left(t_0^2+t_F^2\right)V_{n1}^2V_{n2}^2 + 4\left(t_0^2+2t_F^2\right)V_{n2}^4\cos(\Phi)^2\right),\\
N_{1xy} &= -\frac{4\sin(\Phi)^2\cos(\Phi)^4\left(t_F^2-t_0^2\right)^3 V_{n1}^2 V_{n2}^4}{t_F^6\left(V_{n1}^2\sin(\Phi)^2+V_{n2}^2\cos(\Phi)^2\right)^5}\left(-8t_F^2V_{n1}^6\sin(\Phi)^4 + V_{n1}^4V_{n2}^2\sin(\Phi)^2\left(3t_F^2\sin(\Phi)^2+\left(12t_0^2+13t_F^2\right)\cos(\Phi)^2\right)\right.\\
&\quad \left. - V_{n1}^2V_{n2}^4\cos(\Phi)^2\left(\left(10t_0^2+13t_F^2\right)\sin(\Phi)^2+\left(2t_0^2+t_F^2\right)\cos(\Phi)^2\right) + 2V_{n2}^6\left(2t_0^2+3t_F^2\right)\cos(\Phi)^4\right),\\
N_{2xy} &= -\frac{4\sin(\Phi)^4\cos(\Phi)^2\left(t_F^2-t_0^2\right)^3 V_{n1}^4 V_{n2}^2}{t_F^6\left(V_{n1}^2\sin(\Phi)^2+V_{n2}^2\cos(\Phi)^2\right)^5}\left(-8t_F^2V_{n2}^6\cos(\Phi)^4 + V_{n1}^2V_{n2}^4\cos(\Phi)^2\left(3t_F^2\cos(\Phi)^2+\left(12t_0^2+13t_F^2\right)\sin(\Phi)^2\right)\right.\\
&\quad \left. - V_{n1}^4V_{n2}^2\sin(\Phi)^2\left(\left(10t_0^2+13t_F^2\right)\cos(\Phi)^2+\left(2t_0^2+t_F^2\right)\sin(\Phi)^2\right) + 2V_{n1}^6\left(2t_0^2+3t_F^2\right)\sin(\Phi)^4\right).
\end{aligned}
\tag{B14}
$$

Note that when taking the derivatives for the coefficients N_j and N_{ij}, we need to set the t_F in the coefficients into T shown in eq. (B1) for computation.